Biochimica et Biophysica Acta 1818 (2012) 1884–1894

Contents lists available at SciVerse ScienceDirect

Biochimica et Biophysica Acta

journal homepage: www.elsevier.com/locate/bbamem

Review

Modulation of metabolic communication through gap junction channels by transjunctional voltage; synergistic and antagonistic effects of gating and ionophoresis ☆

Nicolás Palacios-Prado, Feliksas F. Bukauskas *

Dominick P. Purpura Department of Neuroscience, Albert Einstein College of Medicine, Bronx, NY, USA

ARTICLE INFO

Article history:
Received 29 April 2011
Received in revised form 25 August 2011
Accepted 2 September 2011
Available online 10 September 2011

Keywords:
Connexin
Voltage gating
Dye transfer
Heterotypic channel
Signaling asymmetry
Transjunctional permeability and flux

ABSTRACT

Gap junction (GJ) channels assembled from connexin (Cx) proteins provide a structural basis for direct electrical and metabolic cell–cell communication. Here, we focus on gating and permeability properties of Cx43/Cx45 heterotypic GJs exhibiting asymmetries of both voltage-gating and transjunctional flux (J_j) of fluorescent dyes depending on transjunctional voltage (V_j). Relatively small differences in the resting potential of communicating cells can substantially reduce or enhance this flux at relative negativity or positivity on Cx45 side, respectively. Similarly, series of V_j pulses resembling bursts of action potentials (APs) reduce J_j when APs initiate in the cell expressing Cx43 and increase J_j when APs initiate in the cell expressing Cx45. J_j of charged fluorescent dyes is affected by ionophoresis and V_j-gating and the asymmetry of J_j–V_j dependence in heterotypic GJs is enhanced or reduced when ionophoresis and V_j-gating work in a synergistic or antagonistic manner, respectively. Modulation of cell-to-cell transfer of metabolites and signaling molecules by V_j may occur in excitable as well as non-excitable tissues and may be more expressed in the border between normal and pathological regions where intercellular gradients of membrane potential and concentration of ions are substantially altered. This article is part of a Special Issue entitled: The Communicating junctions, composition, structure and characteristics.

Contents

☆ This article is part of a Special Issue entitled: The Communicating junctions, composition, structure and characteristics.

* Corresponding author at: 1300 Morris Park Ave, Bronx, NY 10461, USA. Tel.: +1 718 430 4130; fax: +1 718 430 8944.
E-mail address: feliksas.bukauskas@einstein.yu.edu (F.F. Bukauskas).

0005-2736/$ – see front matter
doi:10.1016/j.bbamem.2011.09.001

1. Introduction

1.1. Connexins, hemichannels and gap junction channels

Direct cell-to-cell electrical and molecular signaling between adjacent cells in virtually all multi-cellular organisms is accomplished through intercellular gap junction (GJ) channels, which in chordates are formed by two oligomerized hexamers of connexin (Cx) proteins called a connexon or hemichannel (HC); the list of most frequently used abbreviations is provided in Table 1. Docking of two HCs form the GJ channel that spans the plasma membranes of adjacent cells and provides a direct pathway for cell-to-cell electrical signaling and metabolic communication allowing the passage of small ions, amino acids, metabolites and signaling molecules such as cAMP, IP_3, 5-HT, siRNA and small peptides ([1–5] and reviewed in [6]). Unapposed/nonjunctional hemichannels (uHCs) from closely apposed cells can dock and form GJ channels with inter-cytoplasmic pores. Individual GJ channels tend to cluster at high density forming a junctional plaque (JP). HCs can be homomeric or heteromeric, depending whether they are composed by the same or different Cx isoforms, respectively. In humans, 21 members of the Cx family have been identified [7], giving a wide diversity of GJ channels. Docking of homomeric HCs formed of the same or different Cx isoforms assembles homotypic or heterotypic GJ channels, respectively, and composing HCs are called as apposed hemichannels (aHCs). If the GJ channel contains at least one heteromeric aHC then we call it a heteromeric GJ channel. Cells in many tissues co-express several Cx isoforms and different homotypic GJ channels can cluster into the same JP forming bi-homotypic GJs [8]. Potentially, 21 Cx isoforms can form 210 different heterotypic GJs. This number increases to thousands for heteromeric GJs if rotational asymmetry of docked aHCs is considered, which can be assembled from two or more co-expressed Cx isoforms.

Earlier studies have shown that heterotypic GJs in which a Cx45 is paired with Cx31, Cx40 or Cx43 exhibit a strong voltage-gating asymmetry and modulatable cell-to-cell electric signaling from nearly unidirectional to bi-directional [9–10]. Cx45 is expressed in a variety of tissues, but most abundantly in cardiovascular and nervous systems [11–12]. Blood vessels express Cx37, Cx40, Cx43 and Cx45, with the most abundant expression of Cx37 and Cx40 in endothelial cells and Cx43 and Cx45 in smooth muscle cells [13–14]. Thus, heterotypic GJs containing Cx45 can be formed between smooth muscle cells as well as between smooth muscle and endothelial cells. Furthermore, Cx45 may form GJs with mCx30.2, Cx40 and Cx43 in the heart between cardiomyocytes or cardiomyocytes and fibroblasts [15], between neurons with mCx30.2 and Cx36 [16] and between astrocytes and neurons with Cx43 [17].

It has been reported that pannexin proteins (vertebrate homologous of invertebrate innexins) may also form intercellular channels in paired oocytes [18], but the formation and function of pannexin-based GJ channels in mammalian cell lines and tissues is yet to be demonstrated [19].

1.2. Connexin compatibility to form homotypic and heterotypic gap junctions

Intercellular communication through GJ channels between identical cell types (homocellular) and different cell types (heterocellular) is universally widespread in multicellular organisms. Different cell types may express the same or different sets of Cxs. While a Cx isoform may be expressed by different cell types, a given cell type may express one or more Cx isoforms. Heterocellular connections and their asymmetric properties were first described in the giant motor synapses of the crayfish in the late 50s [20], but it took thirty years to demonstrate that GJ channels composed by distinct Cx and innexin isoforms were the molecular substrate of rectifying synapses [21–24]. These channels were called hybrid cell–cell channels [21] or heteromolecular channels [22], but the name "heterotypic channels" was coined two years later with a precise demonstration of emergent rectification properties when Cx26 HCs dock with Cx32 HCs [25]. These studies raised the question about the extent of interaction between cell types expressing dissimilar HCs to form functional heterotypic or heteromeric GJ channels. Compatibility between HCs determines whether the same or different cell types may or may not form GJ channels. When heterotypic channels are formed, new electrical and permeability properties may arise [23,25], increasing the scope of possible functions for heterocellular connections. Compatible Cxs play an important role in integrating cells into functional compartments, while incompatible Cxs may participate in delineating boundaries between them. Although compatible Cxs can ensure electrical coupling, a limited Cx-type dependent permeability to metabolites and signaling molecules might be critical for initiation of compartmentalization even in electrically coupled network and formation of distinct tissues and organs during developmental processes [26–27]. Evidence for heterocellular connections and heterotypic GJ channels is abundant, particularly in the eye [28–29], brain [11,30–31], heart [12,32] and cardiovascular system [33–34]. Collected studies performed by us and other groups using a dual whole-cell patch clamp and dye transfer in mammalian cells as well as a dual two-electrode voltage clamp in *Xenopus* oocytes, [6,11,21,25,35–40], allow us to present a table for functional and nonfunctional homotypic and heterotypic pairings (Table 2). Presented data reveals that some Cxs (such as 43 and 45) have the ability to form functional pairings with most of other Cxs, while Cx31 and Cx36 are less compatible. Cxs 23, 25, 33, 39 and 59 have not yet been tested to form heterotypic GJs. From 210 possible heterotypic pairings, only 92 were examined and among them, only 45 form functional channels (Table 2). It still remains to be demonstrated whether nonfunctional pairings have the potential to dock and form physical GJ channels. It has been reported that docking between HCs is strongly determined by the sequence of amino acids and disulfide bond pattern of extracellular loops [35,41–43], but analysis of a number of chimeras suggested that cytoplasmic loop and C-terminus domains may be involved as well [44]. Cxs of the α-group displayed eight

Table 1
The list of most frequently used abbreviations.

Abbreviation	Full name
AF^{350}	Alexa Fluor-350
aHC	Apposed hemichannel
AP	Action potential
Cx	Connexin
FI	Fluorescence intensity
GJ	Gap junction
g_j	Transjunctional conductance
GJC	Gap junctional communication
HC	Hemichannel
I_j	Transjunctional current
J_j	Transjunctional flux
JP	Junctional plaque
K_{asym}	Coupling asymmetry coefficient
LY	Lucifer Yellow
N_o	Number of fully open channels
N_F	Number of operational/functional channels
P_j	Transjunctional permeability
P_P	Permeability from cell-2 to pipette-2
P_γ	Single channel permeability
uHC	Unapposed hemichannel
V_1 and V_2	Voltage in cell-1 and cell-2, respectively
V_h	Holding potential
V_j	Transjunctional voltage
V_m	Transmembrane potential
V_R	Resting potential
W_P	Working point
γ_o	Unitary conductances of GJ channel at the open state
γ_{res}	Unitary conductances of GJ channel at the residual state
$\gamma_{o,H}$	Unitary conductances of aHC at the open state
$\gamma_{res,H}$	Unitary conductances of aHC at the residual state

functional and seven nonfunctional heterotypic pairings. Cxs of the β-group displayed seven functional and six nonfunctional heterotypic pairings. In summary, all Cxs exhibited 15 functional and 13 non-functional intra-group heterotypic pairings, while among inter-group pairings 30 were functional and 32 nonfunctional (Table 2). This data suggest that there is no relation in the ability of Cxs to form functional heterotypic GJs within or between groups [45]. Interestingly, Cxs 23, 29 and 31.1 do not form functional homotypic GJs, and also did not express functional GJs for all ten examined heterotypic pairings. The inability to form functional GJ channels does not necessarily mean nonfunctional uHCs, as recently shown for Cx29 (CX30.2) [46].

2. Gating of GJ channels

2.1. V_m- and V_j-sensitive gating of homotypic GJ channels; two types of voltage gating mechanisms

GJ channels allow electrical signal transfer between cells and this signaling can be modulated by chemical reagents (chemical-gating) and by voltage (voltage-gating) of two types: 1) the transmembrane potential (V_m), and 2) the transjunctional voltage (V_j). All Cx-based GJ channels exhibit sensitivity to V_j, but few are sensitive to V_m at a detectable level. Homotypic GJ channels normally show symmetric steady-state transjunctional conductance (g_j)–V_j relations, except in cases where V_m-sensitivity is present [35,47]. In addition, instantaneous transjunctional current (I_j) that reflect electrical properties of the channel pore at the open state, rectifies in respect to V_j but at a different degree depending on Cx isoform. This rectification is masked in homotypic channels, but can be significant in heterotypic channels when unitary conductances of aHC differ considerably. The electrical properties of aHCs have been historically defined by a two-state Boltzmann distribution dependence on V_j [48], assuming that each aHC possesses one gating mechanism that senses V_j independently of the state of the other gate in series and closes the channel fully. However, measurements at the level of a single GJ channel and uHC in cells expressing wild type Cxs or their mutants strongly enforced a view that both aHC and uHC contain, at least, two voltage-sensitive gating mechanisms, called as the 'fast' gate and "slow" or "loop" gate [49]. Single-channel recordings exhibited not only open and closed states but also substates. Among numerous substates, the one that has the longest dwell-time is called a residual state and typically constitutes 1/4th–1/5th of the open state

Table 2
Compatibility of Cx isoforms to form homotypic and heterotypic GJs. Corresponding mouse and human names for genes and proteins were taken from [45]. Names of mouse (Gj) and human (GJ) genes with corresponding proteins are shown in white and gray squares, respectively. Ability to form functional or non-functional homotypic and heterotypic GJs are indicated by '+' and '−', respectively; '*' stands for disputed conclusions. Data are summarized from reports of different groups based on dye transfer studies and using a dual whole-cell patch clamp in mammalian cells and dual two electrode voltage clamp in Xenopus oocytes [6,11,21,25,35–40].

GENE NAME	PROTEIN NAME	Mouse Human	*Gje1* *GJE1*	*---* *GJB7*	*Gjb2* *GJB2*	*Gjc3* *GJC3*	*Gjb6* *GJB6*	*Gjd3* *GJD3*	*Gjb4* *GJB4*	*Gjb3* *GJB3*	*Gjb5* *GJB5*	*Gjb1* *GJB1*	*Gja6* *---*	*Gjd2* *GJD2*	*Gja4* *GJA4*	*Gjd4* *GJD4*	*Gja5* *GJA5*	*Gja1* *GJA1*	*Gjc1* *GJC1*	*Gja3* *GJA3*	*Gjc2* *GJC2*	*Gja8* *GJA8*	*Gja10* *GJA10*	*---* *GJA9*
GENE NAME	PROTEIN NAME	Mouse Human	**Cx23** CX23	--- CX25	**Cx26** CX26	**Cx29** CX30.2	**Cx30** CX30	**Cx30.2** CX31.9	**Cx30.3** CX30.3	**Cx31** CX31	**Cx31.1** CX31.1	**Cx32** CX32	**Cx33** ---	**Cx36** CX36	**Cx37** CX37	**Cx39** CX40.1	**Cx40** CX40	**Cx43** CX43	**Cx45** CX45	**Cx46** CX46	**Cx47** CX47	**Cx50** CX50	**Cx57** CX62	--- CX59
Mouse Human	Mouse Human																							
Gje1 *GJE1*	**Cx23** CX23		−																					
--- *GJB7*	--- CX25			+																				
Gjb2 *GJB2*	**Cx26** CX26				+																			
Gjc3 *GJC3*	**Cx29** CX30.2					−																		
Gjb6 *GJB6*	**Cx30** CX30				+		+																	
Gjd3 *GJD3*	**Cx30.2** CX31.9							+																
Gjb4 *GJB4*	**Cx30.3** CX30.3						+		+															
Gjb3 *GJB3*	**Cx31** CX31				+		+		−	+														
Gjb5 *GJB5*	**Cx31.1** CX31.1				−				−	−	−													
Gjb1 *GJB1*	**Cx32** CX32				+	−	+	+	−	+	−	+												
Gja6 *---*	**Cx33** ---												+											
Gjd2 *GJD2*	**Cx36** CX36				−		−		−	−	−	−		+										
Gja4 *GJA4*	**Cx37** CX37				−		+		+	−	−	−		+	+									
Gjd4 *GJD4*	**Cx39** CX40.1															*								
Gja5 *GJA5*	**Cx40** CX40				−		+	+	+	−	−	−		−	+		+							
Gja1 *GJA1*	**Cx43** CX43				−		+	+	+	−	−	*		+	+		*	+						
Gjc1 *GJC1*	**Cx45** CX45				+		+	+	−	+	−	+		+	+		+	+	+					
Gja3 *GJA3*	**Cx46** CX46				+				+	−	−	+		−	+		−	+	−	+				
Gjc2 *GJC2*	**Cx47** CX47											+		+				+	+		+			
Gja8 *GJA8*	**Cx50** CX50				+						−	+		−	−		−	−		+		+		
Gja10 *GJA10*	**Cx57** CX62				−		−		+	−	−	−			+		−	+	+	−		−	+	
--- *GJA9*	--- CX59																							

Homotypic:
–Functional, 17
–Nonfunctional, 3
Heterotypic:
–Intra–group functional, 15
–Intra–group nonfunctional, 13
–Inter–group functional, 30
–Inter–group nonfunctional, 32

conductance [49–50]. Transitions between the fully closed state and any other state are slow (>10 ms), whereas any other transition is fast (< 2 ms; presumably much faster without signal filtering) [50]. These time-course studies of state transitions gave rise to names for "fast and slow" gates. Fast- and slow-gating in each HC have a determined polarity of closure or "gating polarity", which means that relative positive or negative V_j or V_m on the cytoplasmic side of gates will increase their probability to close. It is assumed that gating polarities for uHC and aHC are conserved, but the possibility that docking reverse the polarity of gating cannot be excluded. Interestingly, all uHCs studied so far have shown negative gating polarity for the slow-gating mechanism, which is generally less voltage-sensitive than the fast-gating mechanism. Hence, each GJ channel has four V_j-sensitive gating mechanisms in series and they interact in a contingent manner, i.e., voltage across one aHC depends on the state as well as conductance of the aHC in series. The extent of gap junctional communication (GJC) depends not only on V_j sensitivity of those gates, but also on several other factors: 1) a number of GJ channels that open at any given time, 2) unitary conductances of GJ channel at open and residual states (γ_o and γ_{res}, respectively), and 3) perm-selectivity of aHCs. GJC can be modulated by V_j, intracellular ionic composition, posttranslational modifications, and different chemical agents [6]. These factors may vary during pathological conditions, such as hypoxia [51], ischemia [52] or epilepsy [53], causing significant dysregulation of electrical and metabolic GJC. Moreover, GJ channels are sensitive to $[Ca^{2+}]_i$, $[H^+]_i$ and V_j [54] that varies under physiological conditions suggesting that modulation of GJC by these factors may be important for normal cell functions.

2.2. Voltage gating and electrical signal transfer asymmetries in heterotypic GJs

Heterotypic GJ channels typically show asymmetric instantaneous and steady-state g_j–V_j relationships. The former is a property of the conductive pore and can be explained by fast rectification of γ_o and γ_{res} that may be sensitive to V_j and/or V_m [55]. Even under normal conditions and at $V_j = 0$, a fraction of channels are closed at the residual state and therefore their rectification can influence instantaneous g_j–V_j relationship as well [56–57]. In addition, rectification of the channel conductance arises from an asymmetry in the position of charged amino acids near the channel pore surface, explaining the molecular determinants of fast rectification in heterocellular electrical synapses [58]. On the other hand, steady-state g_j–V_j asymmetries can be explained by differences in: 1) V_j sensitivity of fast and slow gating mechanisms of aHCs, 2) unitary conductances of aHCs at the open and residual states ($\gamma_{o,H}$ and $\gamma_{res,H}$, respectively), and 3) gating polarity. There were multiple attempts to determine gating polarity of Cxs by assuming that V_j-gating asymmetry of heterotypic GJs arises from differences in V_j-gating of corresponding homotypic GJs. However, when $\gamma_{o,H}$s are considerably different, the fraction of V_j that drops on the aHC with smaller $\gamma_{o,H}$ is significantly higher resulting to enhanced and reduced V_j-sensitivities of aHCs with smaller and higher $\gamma_{o,H}$s, respectively, compared to those in corresponding homotypic GJs [9,56]. Eventually, changes in V_j-sensitivity of aHCs due to differential drop of V_j lead to marked g_j–V_j asymmetries. For example, in Cx45/Cx43 heterotypic channels due to ~4-fold difference between Cx43 and Cx45 $\gamma_{o,H}$s results in significantly higher V_j-gating asymmetry than that predicted from intrinsic V_j-gating sensitivities of Cx43 and Cx45 [9]. When aHCs exhibit opposite gating polarities, then maximal g_j–V_j asymmetry arises [59–60] because one V_j polarity tends to open both aHCs and the opposite gating polarity tends to close both aHCs.

Our reported and unpublished data show that all heterotypic GJs channels formed on one side from Cx45 and on other side from mCx30.2, Cx31, Cx36, Cx40, Cx43, Cx47 and Cx57 exhibits strong V_j-gating and electrical signal transfer asymmetries. Experiments were performed using a dual whole-cell voltage clamp method (detailed in [10]) in co-cultures of HeLaCx45WT, HeLaCx45-CFP or HeLaCx45-EGFP and HeLa cells stably expressing other partner Cxs of wild type or fused with fluorescent proteins of different colors. Typically, we used co-cultures in which one type of cells expressed Cx fused with EGFP and another type of cells expressed wild type Cx or Cx fused with CFP. Cells expressing non-tagged Cxs were preloaded with DAPI at concentration of ~10 μM for ~0.5 h. This allowed selection of cell pairs expressing different Cxs and exhibiting at least one JP. Some of our data on voltage-gating asymmetry in heterotypic GJs are illustrated in Fig. 1. Fig. 1A shows an example of I_j dynamics measured in HeLaCx45WT cell of HeLaCx31-EGFP/HeLaCx45WT cell pairs in response to slow (0.7 mV/s) V_j ramps applied to Cx31-EGFP expressing cell. Slow V_j ramps allow for continuous measurement of steady-state g_j dependence on V_j as shown in Fig. 1B. The normalized g_j–V_j dependence is strongly asymmetric with a peak of g_j at $V_j \approx -25$ mV. The reduction of g_j at positive V_js is caused by the closure of Cx45 aHCs that gate at relative negativity on their cytoplasmic side [9], whereas the reduction in g_j for negative V_js results from closure of Cx31 aHCs that also gate at relative negativity but are less V_j sensitive than Cx45 aHC [61]. Similar V_j-gating asymmetry was reported for mCx30.2/Cx45 [15], Cx40/Cx45 [10], Cx43/Cx45 [9] and Cx57/Cx45 [62] GJs and observed in Cx36/Cx45 and Cx47/Cx45 GJs (unpublished data, F.F.B.).

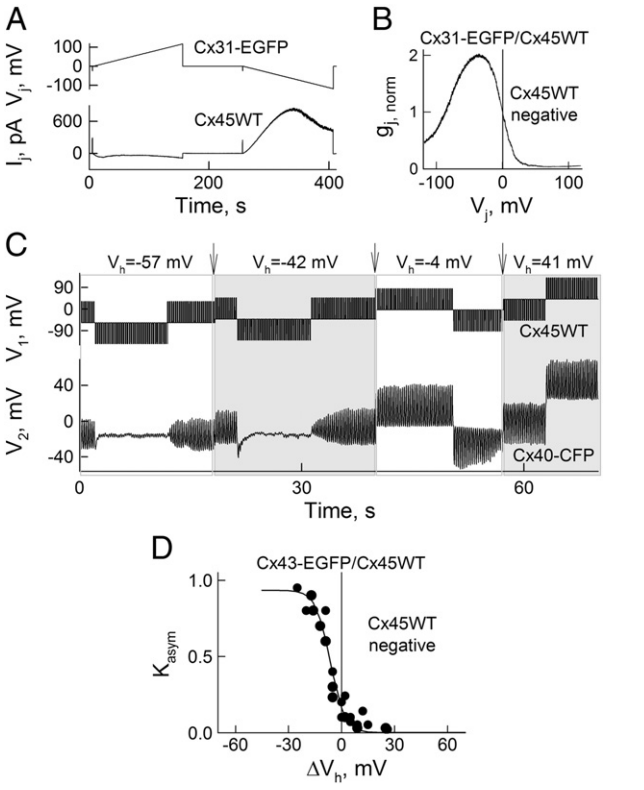

Fig. 1. Asymmetries of V_j-gating and electrical signal transfer in heterotypic junctions formed from Cx45WT paired with Cx31-EGFP, Cx40-CFP and Cx43-EGFP. (A) Example of an I_j recording in response to long V_j ramps (~0.8 mV/s) from 0 to +115 mV and −115 mV applied to the HeLaCx45 cell of a HeLaCx31-EGFP/HelaCx45WT cell pair. (B) Normalized g_j–V_j plot, calculated from the record shown in A, demonstrates gating asymmetry. (C) An example of electrical signal transfer asymmetry in HeLaCx31-EGFP/HeLaCx45WT cell pair; $g_j = 1.4$ nS. Initially HeLaCx45WT cell (cell-1) was voltage clamped at −57 mV and stepped by ±90 mV for 90 ms with 170 ms between pulses. The cell-2 was maintained in current clamp mode, which allowed the recording of electrotonic potentials evoked by repeated voltage steps applied to cell-1. The initial set of depolarizing and hyperpolarizing voltage pulses (0–18 s) shows substantial asymmetry in the amplitudes of responses in cell-2 depending on the polarity of the pulses. Stepwise depolarization of the holding potential of cell-1 (see arrows) leads to a reduction in the degree of signal transfer asymmetry. (D). Normalized dependence of electrical coupling asymmetry coefficient, K_{asym}, on ΔV_h measured in six HeLaCx43-EGFP/HeLaCx45WT cell pairs, where $\Delta V_h = V_{h1} - V_{h2}$.
Adapted from Refs. [9–10,61].

Earlier, it was shown that V_j-gating asymmetry in Cx43/Cx45 GJs can cause asymmetry of electrical signal transfer which can be effectively modulated by the difference in holding potentials between the cells (ΔV_h) [9]. Fig. 1C shows an experiment in which the HeLaCx45WT cell (cell-1) was paired with a HeLaCx40-CFP cell (cell-2); $g_j = 1.4$ nS. Initially cell-1 was voltage clamped at −57 mV and stepped to ±90 mV for 90 ms with 170 ms between pulses. The cell-2 was maintained in current clamp mode, which allowed the recording of electrotonic potentials evoked by repeated voltage steps applied to cell-1. The initial set of depolarizing and hyperpolarizing voltage pulses (0–18 s) shows substantial asymmetry in the amplitudes of responses in cell-2 depending on the polarity of the pulses. During application of +90 mV pulses to cell-1, the amplitude of electrotonic responses in cell-2 (V_2) was ~28 mV; i.e., the coupling coefficient for signal transfer, $k_{1\to 2,+90} = V_2/V_1 = 28/90 = \sim 0.3$. During application of −90 mV pulses, the $V_2 \approx 0.3$ mV and $k_{1\to 2,-90} \approx 0.01$. We defined the ratio of coupling coefficients for positive and negative V_j pulses, $k_{1-2,-90}/k_{1-2,+90}$, as the electrical coupling asymmetry coefficient, K_{asym}, which during 0–18 s period was equal ~0.03. Positive pulses were effectively transferred to cell-2, whereas transfer of negative pulses was greatly attenuated. Transfer of negative pulses gradually decreased due to decrease in g_j. Stepwise increase in the holding potential of cell-1 (see arrows) from −57 mV to 41 mV leads to a gradual increase in K_{asym} by reaching ~1, which stands for symmetric signal transfer. A similar electrical signal transfer asymmetry, which can be modulated from virtually unidirectional to bidirectional by relatively small changes in ΔV_h was reported in Cx31/Cx45 and Cx43/Cx45 GJs [9,61] and observed in Cx36/Cx45 and Cx47/Cx45 GJs expressed in HeLa cells (unpublished, F.F.B.) as well as in amphibian blastomeres exhibiting a small offset in resting potentials [63]. Fig. 1D shows summarized data illustrating K_{asym} dependence on ΔV_h measured in HeLaCx43-EGFP/HeLaCx45WT cell pairs originally reported in [9], were $\Delta V_h = V_{h1} - V_{h2}$. K_{asym} varied from near 1, when the Cx45-expressing cell was more positive, to ~0, when the Cx45 cell was more negative. We observed similar $K_{asym} - \Delta V_h$ dependence in Cx31/Cx45, Cx40/Cx45 and Cx36/Cx45 GJs. In summary, collected data show that ΔV_h significantly modulates electrical signaling asymmetry through several types of heterotypic GJs. This asymmetry increases making Cx45 cell relatively more negative relative to the partner Cx. $K_{asym} - \Delta V_h$ dependence remains the same independent of whether the Cx45- or partner-Cx-expressing cell was stimulated.

3. Dye transfer modulation by transjunctional voltage

It is well established that GJs are permeable to second messengers, such as Ca^{2+}, cAMP and IP_3 in a Cx type dependent manner [6]. For example, Cx43 GJs demonstrate ~15-fold higher permeability than Cx32 GJs for glutamate, glutathione, ADP and AMP, and ~10-fold lesser permeability to adenosine [64]. All of the above-mentioned molecules are comparable in molecular mass and net electric charge with Alexa Fluor-350 (AF^{350}; MW = 326 Da, z = −1) and Lucifer Yellow (LY; MW = 443, z = −2) used in our studies. Here we focus on modulation of cell-to-cell transfer of these dyes by V_j. We did not assess permeability to positively charged dyes because of their strong binding to nucleic acids.

Cx isoforms exhibit different transjunctional permeability (P_j) to the same compound, which for some Cxs can differ by 1000-fold [65]. Single channel permeability (P_γ) is not necessarily proportional to single channel conductance or pore diameter [64,66]. In addition, the fast V_j-sensitive gating mechanism operates as a selectivity filter restricting metabolic cell–cell communication while preserving electrical coupling. It was shown that at the residual state Cx43 and Cx46 GJs are not permeable to fluorescent molecules and cAMP, which permeate the open/main state [67–68]. Therefore, when the fast gate closes to the residual state it narrows the channel pore to the size comparable with the size of atomic ions. For example, P_j of cAMP should be proportional to the number of fully open channels (N_o) at any given time or $g_{j,o} = N_o \cdot \gamma_o$ but not to a total junctional conductance, $g_j = N_o \cdot \gamma_o + (N_F - N_o) \cdot \gamma_{res}$, where N_F is a number all operational/functional channels, and γ_o and γ_{res} are unitary conductances at open and residual states, respectively. As indicated above, even under normal conditions and $V_j = 0$ fraction of GJs can be closed to the residual state. As a result, P_j–V_j relation for molecules (more complex than atomic ions) will be slightly different from g_j–V_j relation due to the 'zero-permeability' of the residual state. In case of charged molecules, an electric field generated by V_j will affect not only V_j-gating but also the motion of charged molecules by ionophoresis, i.e. positively charged molecules move towards a relative negative cell (cathode) and *v.v.* Thus, J_j is affected by both V_j-gating and ionophoresis.

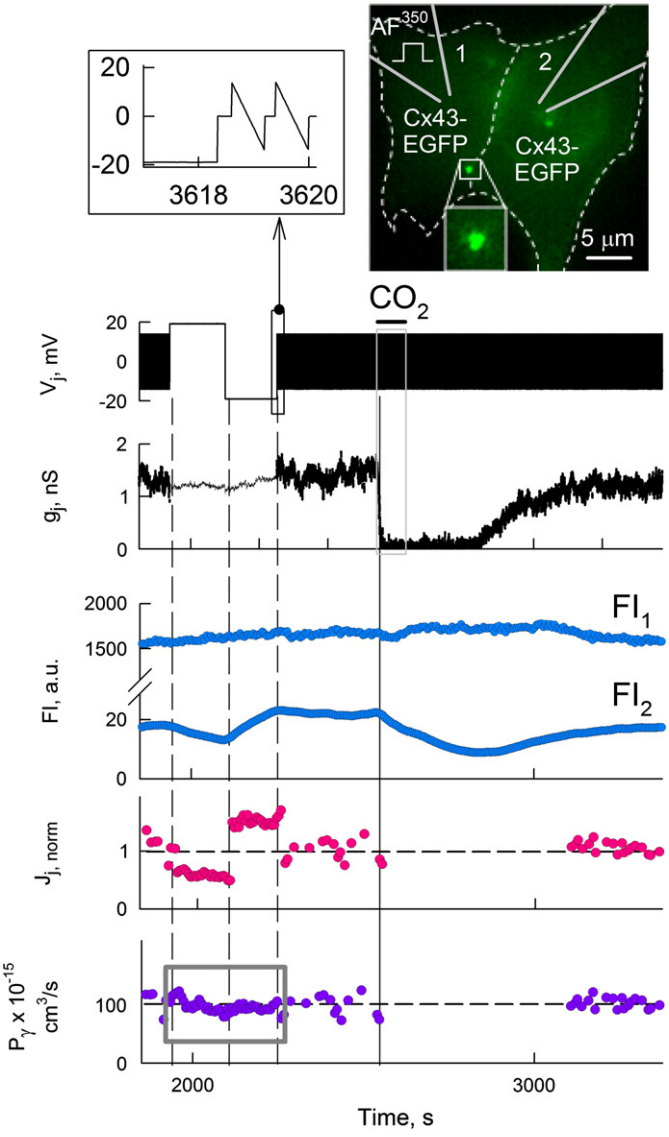

Fig. 2. Dye transfer modulation by ionophoretic effect of V_j in the absence of V_j-gating. A diagram of the experimental setting is superimposed with a fluorescence image of a HeLaCx43-EGFP cell pair exhibiting a single JP (see the inset). The V_j trace shows the voltage protocol applied to cell-1 loaded with AF^{350}. Repeated V_j ramps of ±15 mV applied in cell-1 were used to measure I_j in between V_j steps of ±20 mV (see expanded traces in the inset). FI_1 and FI_2 traces show dynamics of dye fluorescence in cell-1 and cell-2, respectively. $J_{j,\,norm}$ and P_γ traces show AF^{350} flux normalized to the control value, and single channel permeability, respectively. Application of CO_2 (horizontal bar) was used to block GJs and calculate P_p, which in this experiment was equal $\sim 1.3 \times 10^{-11}$ cm^3/s.
Adapted from Ref. [54].

3.1. Theoretical and methodological aspects in estimation of dye flux through GJ channels

To study P_j and transjunctional flux (J_j) dependence on V_j, we used combined dual whole-cell patch clamp and fluorescent imaging methods, described in more detail in [54,62,65]. In brief, pipette-1 and pipette-2 are patched to cell-1 and cell-2, respectively. For J_j measurements, only pipette-1 contained dye of interest, therefore, cell-1 acted as "dye-donor" and cell-2 as "dye-recipient". Typically, patch opening in pipette-1 resulted in a rapid dye loading in cell-1 until reaching saturation. Dye transfer from cell-1 to cell-2 followed by dye diffusion to pipette-2. Therefore, we needed to account for a dye loss in cell-2 due its "leakage" to pipette-2 that was not part of equations used to analyze P_j and J_j.

Assuming that Goldman–Hodgkin–Katz (GHK) equation [69] applies to J_j, then it can be expressed through P_j multiplied by the driving force, which for a charged molecule involves the gradients of both chemical and electrical potentials:

$$J_j = \frac{P_j\left(zFV_j/RT\right)\left[C_1 - C_2\exp\left(-zFV_j/RT\right)\right]}{\left[1-\exp\left(-zFV_j/RT\right)\right]} \quad (1)$$

where z is the net electric charge of the dye molecule, F is Faraday's constant, R is the gas constant, T is the absolute temperature, and C_1 and C_2 are dye concentrations in cell-1 and cell-2, respectively.

As proposed earlier [1], J_j can be described in differential terms as follows: $J_j = \mathrm{vol}_2(\Delta C_2/\Delta t)$, where, vol_2 is the volume of cell-2 and ΔC_2 is a change in dye concentration in cell-2 during the time interval, Δt. If to account an effect of dye loss to pipette-2 with permeability P_p then

$$J_j = vol_2(\Delta C_2/\Delta t) + P_p C_2. \quad (2)$$

Substituting in Eq. (1) an expression of J_j shown by Eq. (2), we come to the following expression of P_j:

$$P_j = \frac{\left[vol_2(\Delta C_2/\Delta t) + P_p C_2\right]\left[1-\exp\left(-zFV_j/RT\right)\right]}{\left(zFV_j/RT\right)\left[C_1 - C_2\exp\left(-zFV_j/RT\right)\right]}. \quad (3)$$

Based on our studies as well as others [70–71], we assumed that when the concentration of a fluorescent dye is below 1 mM, C_1 and C_2 are directly proportional to fluorescence intensities in cell-1 (FI_1) and cell-2 (FI_2), i.e., $C_1 = k\ FI_1$ and $C_2 = k\ FI_2$, where k is a constant. Then, Eq. (3) can be expressed as follows:

$$P_j = \frac{\left[vol_2(\Delta FI_2/\Delta t) + P_p FI_2\right]\left[1-\exp\left(-zFV_j/RT\right)\right]}{\left(zFV_j/RT\right)\left[FI_1 - FI_2\exp\left(-zFV_j/RT\right)\right]} \quad (4)$$

where $\Delta FI_2 = FI_{2(n+1)} - FI_{2(n)}$ is the change in FI_2 over the time, $\Delta t = (t_{n+1} - t_n)$; n is nth time point in the recording. In the absence of a voltage gradient, permeability at $V_j = 0$ ($P_{j,0}$) can be expressed as follows:

$$P_{j,0} = \frac{\left[vol_2(\Delta FI_2/\Delta t) + P_p FI_2\right]}{\left[FI_1 - FI_2\right]}. \quad (5)$$

To estimate P_p, we uncoupled cells by using 100% CO_2 or long chain alkanols and measured kinetics of FI_2 decay over time reflecting a leakage of dye from cell-2 to pipette-2. Under blocking conditions, $P_{j,0} = 0$, therefore from the Eq. (5) follows that:

$$P_p = \frac{-\ vol_2\ (\Delta FI_2/\Delta t)}{FI_2}. \quad (6)$$

Our data show that P_p can vary in the range of 1.1 to 4×10^{-11} cm^3/s. In this equation, it was assumed that the concentration of dye in pipette-2 is negligible. This assumption may not be very true, specifically for pipettes with long tapered tips. For this reason, we always made pipettes with tapered tips as short as possible. P_p depends mainly on the size of the open patch at the tip of the pipette, which can vary among experiments. Therefore, its value should be estimated in each experiment. If approximation of P_j and J_j decay under uncoupling conditions approached zero then this supported a notion that P_p estimates were reliable.

In all permeability studies we have used negatively charged dyes that show relatively low binding to cytoplasmic components. In separate studies, we have permeabilized cells preloaded with AF^{350} and LY for ~1 h. They revealed that fluorescence of AF^{350} over ~5 min decayed almost completely, while LY revealed some residual fluorescence of ~10%. Similar control experiments were performed by Ek-Vitorin and Burt [71], in which RinCx43 cells were loaded with NBD-M-TMA for ~35 min, and 6 min after permeabilization with β-escin, dye fluorescence was undetectable. Based on these experiments, we can assume that the error in our evaluations of P_js could be ~10% for LY and negligible for AF^{350}. In addition, obtained P_j and P_γ values, shown in Figs. 2, 4 and 5, were relatively constant over the time course of experiments indicating that binding of AF^{350}

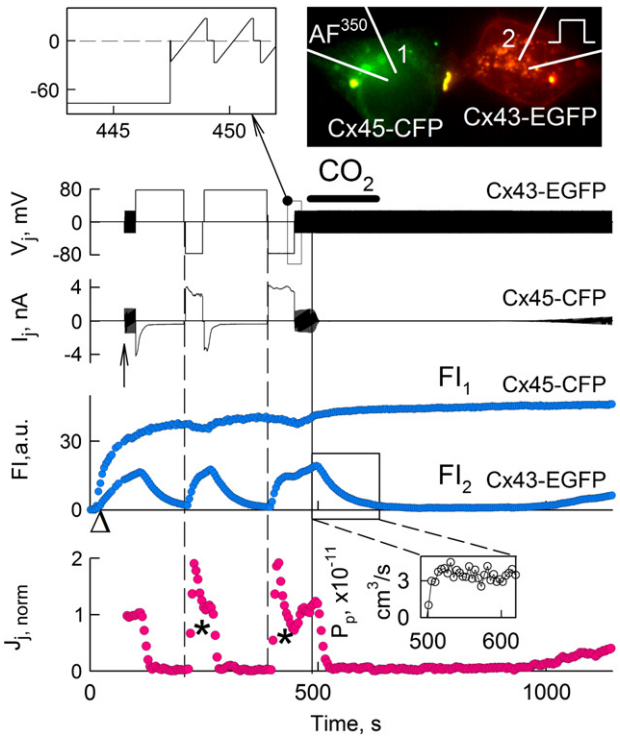

Fig. 3. Dye transfer modulation by V_j steps in a HeLaCx43-EGFP/HeLaCx45-CFP cell pair shown in the top-right diagram. V_j was applied to the Cx43-EGFP expressing cell, while the Cx45-CFP expressing cell was loaded with AF^{350}. Repeated V_j ramps of ±25 mV applied before and after voltage steps of ±80 mV (top-left inset) were used to measure I_j. FI_1 and FI_2 traces show the dynamics of AF^{350} fluorescence in cell-1 and cell-2, respectively. CO_2 application (horizontal bar) was used to block GJs and calculate P_p (bottom-right inset). The $J_{j,norm}$ trace shows the normalized total junctional flux. Δ sign on FI trace and arrow on I_j trace indicate moments of patch opening in cell-1 and cell-2, respectively.
Adapted from Ref. [54].

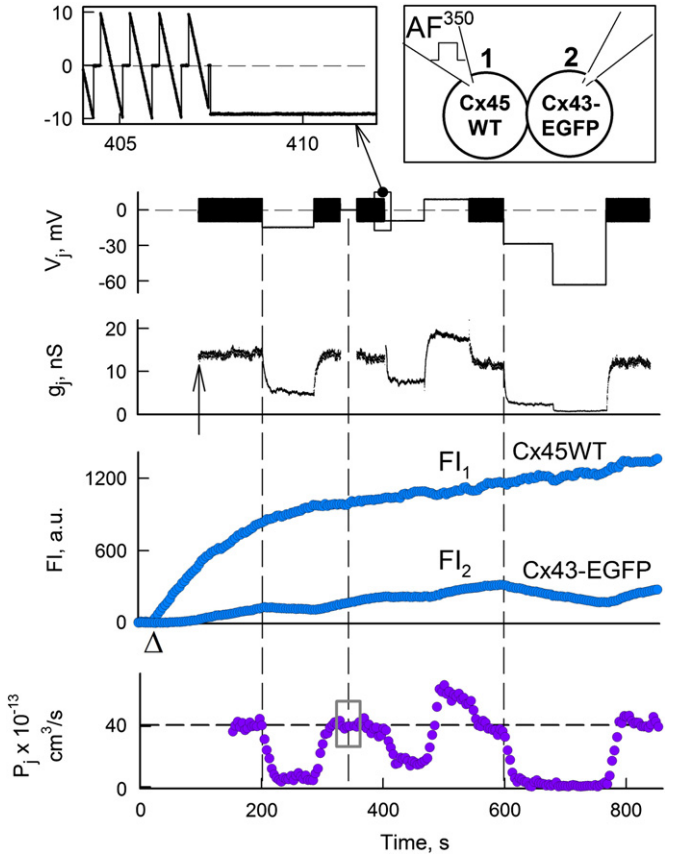

Fig. 4. Dye transfer modulation by small V_js. Electrophysiological and fluorescence imaging recordings in a HeLaCx43-EGFP/HeLaCx45WT cell pair. V_j trace shows the voltage protocol applied to the Cx45-expressing cell (loaded with AF^{350}, see top-right diagram). Repeated V_j ramps of ±10 mV (top-left inset) were used to measure g_j in between V_j steps. FI_1 and FI_2 are fluorescence intensities measured in cell-1 and cell-2, respectively. The P_j trace shows the total junctional permeability. On average, during repeated small amplitude V_j ramps, $P_j = \sim 39.6 \times 10^{-13}$ cm^3/s (horizontal dotted line). Δ sign on FI trace and arrow on I_j trace indicate moments of patch opening in cell-1 and cell-2, respectively.
Adapted from Ref. [54].

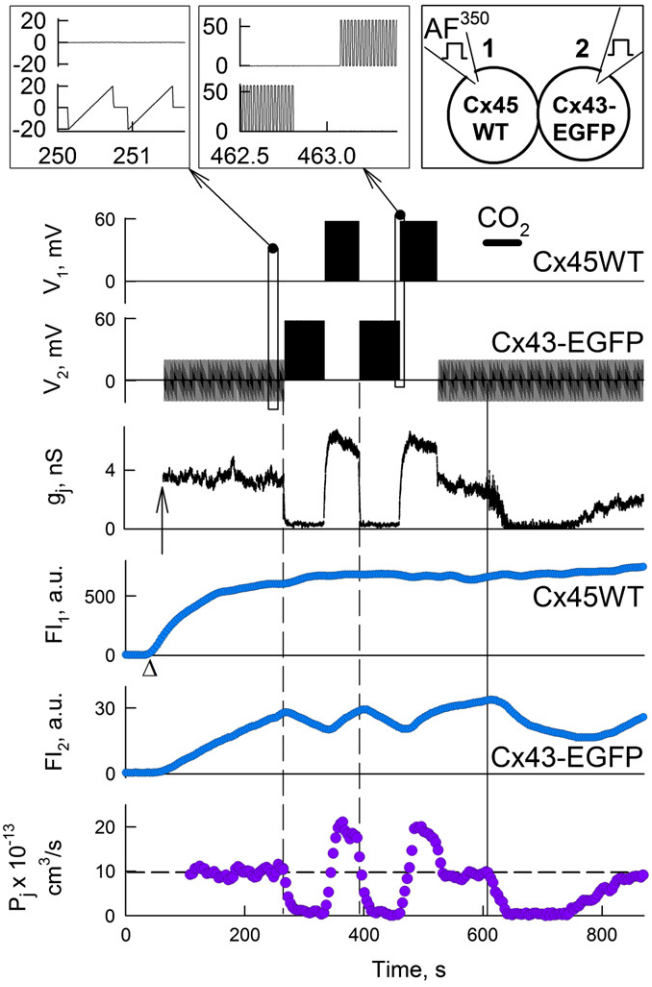

Fig. 5. Dye transfer modulation by bursts of +60 mV pulses 10 ms in duration repeated at 50 Hz frequency (top-middle inset), and applied alternately to cell-1 and cell-2 of a HeLaCx43-EGFP/HeLaCx45WT cell pair (top-right diagram). V_1 and V_2 traces show voltage protocols applied in cell-1 (loaded with AF^{350}) and cell-2, respectively. Repeated V_j ramps of ±20 mV applied in cell-2 (top-left inset) were used to measured I_j and calculate the g_j trace. FI_1 and FI_2 traces show dynamics of dye fluorescence in cell-1 and cell-2, respectively. The P_j trace shows the total junctional permeability. On average, at $V_j = 0$ mV, $P_j = \sim 9.9 \times 10^{-13}$ cm^3/s (horizontal dotted line). During series of pulses, P_j was calculated using Eq. (**2**) at $V_j = 21$ mV. CO_2 application (horizontal bar) was used to block GJs and calculate P_p. Δ sign on FI trace and arrow on I_j trace indicate moments of patch opening in cell-1 and cell-2, respectively.
Adapted from Ref. [54].

does not add a significant error to the absolute values of calculated permeability.

An estimation of vol_2 was based on the assumption that cells have the shape of a hemisphere. The diameter of a hemisphere was determined by averaging the longest and the shortest diameters of the cell; on average, the volume of examined HeLa cells was ~1800 μm^3. In J_j and P_j evaluations, we neglected dye loss through the non-junctional plasma membrane of cell-2 due to earlier reports showing that dye diffusion through HCs or other non-Cx-related mechanisms is at least ~10-fold lower than dye diffusion to the patch-pipette [65].

Single channel permeability (P_γ) can be found by dividing P_j by the number of fully open channels at any given time, $N_o = g_j/\gamma_o$. For example, P_γ can be found from Eq. (7) as follows:

$$P_\gamma = \frac{\gamma_o\left[(vol_2 \Delta FI_2/\Delta t) + P_p FI_2\right]\ \left[1 - \exp\left(-zFV_j/RT\right)\right]}{g_j\left(zFV_j/RT\right)\ \left[FI_1 - FI_2 \exp\left(-zFV_j/RT\right)\right]}. \quad (7)$$

To increase dye detection sensitivity, which is particularly important in cases where coupling is weak and/or channel permeability is low, time-lapse imaging of fluorescence was performed as follows: the whole visible field was exposed to excitation light to measure FI_1, followed by focused excitation light with a diameter of ~10 μm and directed only at the dye-recipient cell-2 to measure FI_2. The latter allowed to avoid emission light scattering from the dye-donor cell-1 as well as from the dye-filled pipette-1 which can obscure dye transfer to the recipient cell in cases where permeability is low or give the appearance of dye transfer when it is, in fact, absent. Our estimates show that using this approach the sensitivity of dye transfer measurements increases over 100-fold when compared with traditional methods when both cells were exposed to the excitation light.

To minimize dye bleaching, we performed time-lapse imaging exposing cells to a low-intensity light for ~0.5 s every 6 s or more. We also used low dye concentrations in the pipette solution, typically 0.1 mM and below, which minimized photo toxicity, but still provided satisfactory fluorescence intensities [54,62,65].

3.2. Experimental analysis of dye transfer modulation by ionophoresis

To determine the direct effect of a transjunctional electric field on the cell-to-cell transfer of charged dye molecules, we performed studies in HeLaCx43-EGFP cells (Fig. 2), which exhibit reduced sensitivity to V_j

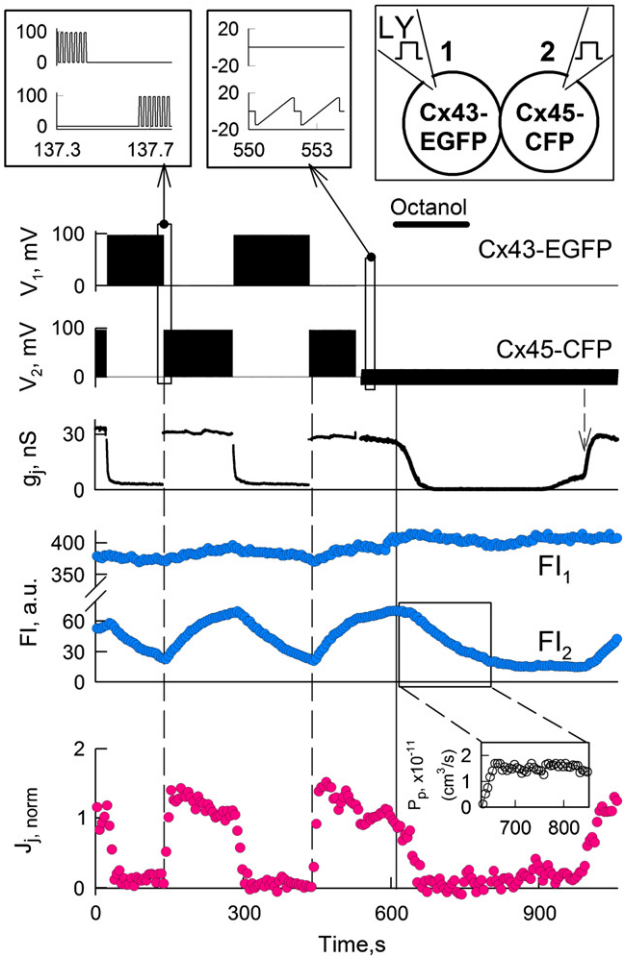

Fig. 6. Lucifer yellow (LY) transfer modulation by bursts of +100 mV pulses 10 ms in duration repeated at 50 Hz frequency (top-left inset), and applied alternately to cell-1 and cell-2 of a HeLaCx43-EGFP/HeLaCx45-CFP cell pair (top-right diagram). V_1 and V_2 traces show voltage protocols applied in cell-1 (loaded with LY) and cell-2, respectively. Repeated V_j ramps of ±14 mV applied in cell-2 (top-middle inset) were used to measured I_j and calculate the g_j trace. FI_1 and FI_2 traces show dynamics of dye fluorescence in cell-1 and cell-2, respectively. The J_j trace shows the total junctional flux calculated with Eq. (2). Octanol application (horizontal bar) was used to block GJs and estimate P_p that was equal ~$1.7 \cdot 10^{-11}$ cm^3/s (bottom-right inset).
Adapted from Ref. [54].

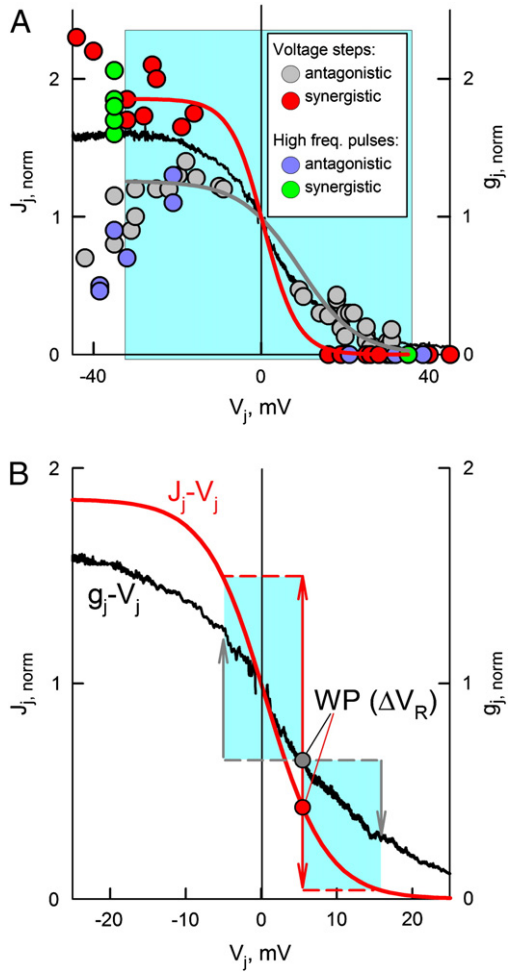

Fig. 7. Modulation of g_j and J_j for AF^{350} by V_j. (A) Summarized data of steady state J_j–V_j for AF^{350} measurements in Cx43/Cx45 cell pairs. Overlap of actual data (circles) and fitting curves using sigmoidal equation for synergistic (red) and antagonistic (gray) J_j–V_j dependences. Data were normalized at $V_j = 0$ mV. Red and gray curves show fitting of the data encompassed in the cyan square and shown in red and gray circles, respectively. Green (synergistic) and blue (antagonistic) filled circles indicate experimental data in which high frequency bursts of pulses of positive polarity were applied to either cell of the cell pair (V_j was positive when the Cx43 cell was stimulated and negative when the Cx45 cell was stimulated, see Fig. 5). The black line shows normalized g_j–V_j plot, averaged from 5 experiments. (B) The figure illustrates how the shift of the working point (WP; gray and red filled circles for g_j and J_j, respectively) along the V_j axis for ±10 mV (cyan rectangles) results in changes of g_j and J_j shown by the vertical arrows. The black and red curves are from A. The changes in g_j are accompanied by relatively larger changes in J_j due to the ionophoretic effect of V_j on the diffusion of charged molecules. Adapted from Ref. [54].

due to a lack of the fast gating mechanism [72]. Cell-1 was loaded with negatively charged AF^{350}. After both cells were transferred to whole-cell mode and FI of AF^{350} in both cells approached a steady state, CO_2 was applied to block GJs to evaluate P_p. I_j and g_j were measured by applying repeated small voltage ramps and V_j steps of ±20 mV to cell-1. The amplitude and duration of the steps were too small to induce reduction in g_j by V_j-gating, while FI_2 exhibited changes due to the direct effect of V_j on AF^{350} transfer. $J_{j,norm}$ trace (calculated using Eq. (2) and normalized to J_j measured just before the first positive V_j step) show that positive V_j step caused a ~60% reduction, while negative V_j steps caused a ~30% increase in $J_{j,norm}$. Despite changes in $J_{j,norm}$, P_γ (calculated using Eq. (7)) remained constant during V_j steps (values boxed into gray square in Fig. 2) and was equal to $82.6 \pm 4.8 \times 10^{-15}$ cm^3/s, which is close to the P_γ previously reported for Cx43-EGFP [65]. A constant P_γ before and during V_j steps is expected because P_γ is a property of the channel and should not depend on V_j if channel pore size and conductance do not change substantially at different V_js due to rectification. Obtained data support a notion that used GHK formalism is indeed applicable to describe P_j for at least V_js of ~±20 mV. Therefore, dye transfer can be accelerated or decelerated by ionophoresis, while P_γ remains unaffected in the absence of V_j-gating.

3.3.1. *V_j-dependent modulation of dye transfer by voltage gating and ionophoresis*

All GJs exhibit V_j-gating with Cx-type dependent sensitivity to V_j. It is evident that V_j-mediated reduction of open probability of GJ channels should reduce P_j. Less obvious is how V_j-gating asymmetry observed in heterotypic GJs (Fig. 1B) affects permeability and whether it leads to a similar or different asymmetry of J_j–V_j and P_j–V_j dependencies.

An example of combined electrophysiological and fluorescence imaging recordings in a Cx43-EGFP/Cx45-CFP cell pair is shown in Fig. 3. Initially, the patch was opened in pipette-1 loaded with AF^{350}. Approximately 1 min later, the patch was opened in pipette-2 (arrow) and repeated ramps of ±25 mV were applied to measure g_j, which initially was ~50 nS. V_j steps of +80 mV applied to Cx43-EGFP cell rapidly reduced I_j, and consequently, g_j dropped to ~5 nS. V_j steps of −80 mV recovered g_j to ~50 nS. CO_2 application for ~2 min induced transient uncoupling and we used FI_2 changes after CO_2 application to evaluate

P_p (Eq. (6)), which was equal $3.8 \cdot 10^{-11}$ cm^3/s. J_j was calculated using Eq. (2) and normalized with $J_{j,o}$ measured just before the first V_j step. During V_j steps of +80 mV, $J_{j,norm}$ declined to zero even though cells remained coupled (~5 nS) and positive V_js applied on Cx43-EGFP side should accelerate transfer of negatively charged AF^{350} molecules. This suggests that positive V_j steps drove GJs to a non-permeable substate. During −80 mV V_j steps, the slow decrease in $J_{j,norm}$ (asterisks) is due to the reduction in concentration gradient of AF^{350}. Data collected in eight other Cx43/Cx45 cell pairs show that dye flux exhibits high levels of asymmetry depending on V_j resembling an asymmetry of V_j-gating. In addition, I_j does not reach a zero level during +80 mV V_j steps presumably due to the inability of the fast gating mechanism to close the GJ channel fully [49]. Earlier, it was reported that GJ channels closed to the residual state become impermeable to AF^{350}, Lucifer yellow (LY) and cAMP, while remaining permeable to small ions, major charge carriers for electrical cell–cell coupling [67–68]. In concert with those reports, in Fig. 3, $J_{j,norm}$ reached a zero level despite the fact that g_j is still ~5 nS.

3.3.2. How effectively V_j can influence dye transfer?

In excitable tissues, relatively high V_js can be expected during action potentials (AP) of ~100 mV in amplitude that can close V_j-sensitive gates and consequently change J_j. However, a major fraction of Cxs in organisms are expressed in non-excitable tissues where changes in the resting potentials (V_R) is the only source for V_j and expected to be much below the amplitude of APs. V_R can vary among cell types and within the same cell type [73] under normal conditions and substantially more under ischemic and other pathological conditions. Therefore, we found it rational to test whether relatively small V_j of ~10 mV or less can modulate P_j in Cx43/Cx45 heterotypic GJs. To answer this question, we examined P_j for AF^{350} by applying relatively small V_j steps (Fig. 4). Repeated V_j ramps of ±10 mV revealed that initial g_j was ~14 nS. Consecutive V_j steps of −14, −9, +9, −30 and −60 mV elicited V_j-gating and modulation of P_j. After ~330 s, V_j ramps were not applied for ~30 s to verify that they did not affect P_j (gray square on P_j trace). During all V_j steps of negative polarity g_j decreased but some residual conductance still remained while P_j decreased even more. During a V_j step of +9 mV, g_j and P_j increased ~30%. From P_j and g_j measurements at the beginning of the record and assuming that for Cx43/Cx45 channels $\gamma_o = 55$ pS [9], we found that $P_{\gamma,Cx43/Cx45} = P_j(\gamma_o/g_j) = \sim 15 \times 10^{-15}$ cm^3/s, which is in good agreement with earlier estimates of single Cx43/Cx45 channel permeability at $V_j \approx 0$ mV [65].

3.4. Dye transfer modulation by V_j pulses resembling bursts of action potentials

In these experiments, we used only positive pulses since APs generated by excitable cells are generally positive, and we examined P_j during stimulation of either cell expressing Cx45 or Cx43. Cell-1 expressing Cx45 was loaded with AF^{350} (see diagram in Fig. 5). Initially, repeated small ramps were applied in cell-2 to measure g_j, which was ~3.5 nS. In response to repeated (50 Hz) pulses of 60 mV in amplitude and 10 ms in duration applied to cell-2, g_j decayed over a ~4 s period and reached a steady state of ~0.2 nS. Subsequently, when a burst of pulses was applied to cell-1, g_j increased to ~6 nS. To find P_p, cells were fully uncoupled with a short application of CO_2. Under control conditions, $P_j \approx 10 \times 10^{-15}$ cm^3/s. To explain 1.9-fold increase in P_j (see P_j trace during stimulation of cell-1), we found, using Eq. (4), that a burst of +60 mV pulses causes the same effect as could cause V_j steps of 21 mV, i.e., ~35% of 60 mV pulses. Single channel permeability estimates in this experiment using the same procedure as we did for data shown in Fig. 4 resulted to $P_{\gamma,Cx43/Cx45} = \sim 14 \times 10^{-15}$ cm^3/s, which is close to values obtained from Fig. 4 and reported earlier for $V_j \approx 0$ mV [65].

Thus, relatively high frequency stimulation of the Cx43-EGFP expressing cell blocked AF^{350} transfer whereas stimulation of the Cx45 expressing cell increased both g_j and P_j equally that presumes linear relationship between P_j and N_F. Similar data were obtained in five other Cx43/Cx45 cell pairs by using AF^{350}. Comparable results were obtained in Cx43-EGFP/Cx45-CFP cell pairs using equivalent experiment protocol to one shown in Fig. 5, but was examined cell–cell transfer of LY instead of AF^{350} (Fig. 6). In summary, these data allow to assume that cell–cell transfer of metabolites in Cx43/Cx45 GJs can be enhanced or reduced depending whether the burst of APs starts in the cell expressing Cx43 or Cx45.

3.5. Synergistic and antagonistic action of V_j-gating and ionophoresis on metabolic communication

Obtained data show that at least in Cx43/Cx45 junctions, V_js as low as ~10 mV can substantially modulate transfer of metabolites of ~400 Da comparable in size with the dyes used (Fig. 4). This modulation of charged molecules can be amplified or reduced depending on whether V_j-gating and ionophoresis act synergistically or antagonistically, respectively. If a Cx43-expressing cell is loaded with a negatively charged dye, i.e., AF^{350}, and subjected to positive or negative V_j steps, then g_j should be reduced or increased and V_j should decelerate or accelerate transfer of AF^{350}, respectively. Thus, at both V_j polarities, V_j-gating and ionophoresis should act on dye transfer synergistically. On the contrary, if a Cx45-expressing cell is loaded with AF^{350}, then V_j-gating and ionophoresis should affect dye transfer antagonistically. Data summarized from 24 cell pairs in Fig. 7 show the synergistic and antagonistic normalized J_j–V_j dependencies observed when cells expressing Cx43 or Cx45, respectively, were loaded with AF^{350}; data were normalized in respect to J_j at $V_j \approx 0$ mV. Red (synergistic) and gray (antagonistic) circles and corresponding fitting curves using sigmoidal equation summarize experiments in which V_j steps of negative or positive polarity were applied to either cell of the pair. From fitting curves, we can find that $\Delta J_j/\Delta V_j$ at $V_j \approx 0$ mV was equal to ~−0.09 and −0.03 normalized units of J_j per mV for synergistic and antagonistic dependencies, respectively. The black curve shows the normalized g_j–V_j dependence averaged from five g_j–V_j plots from which we can find that $\Delta g_j/\Delta V_j$ at $V_j \approx 0$ mV was equal to ~ −0.06 mV^{-1}. Thus, synergistic J_j–V_j dependence was steeper and antagonistic one was shallower than g_j–V_j dependence at $V_j \approx 0$ mV. Green (synergistic) and blue (antagonistic) circles in Fig. 7A indicate experimental data in which burst of pulses of positive polarity were applied to either cell of the cell pair (V_j positive when Cx43 cell was stimulated and *v.v.*). Data shown in green and blue circles were not included in the fitting process but, in general, they show that application of V_j steps or bursts of pulses result in similar effects on J_j.

If ΔV_R is positioned on a g_j–V_j plot of Cx43/Cx45 heterotypic junction as the working point (WP), then changing V_Rs in cell-1 and/or cell-2 would move the WP along the V_j axis and cause substantial changes in g_j and J_j. Fig. 7B illustrates that V_js as small as ±10 mV around the working point of $\Delta V_R = 5$ mV causes ~50% higher changes in J_j than in g_j due to synergistic action of V_j-gating and ionophoresis.

4. Concluding remarks

Collected data demonstrate that V_j can effectively regulate cell–cell transfer of electrical signals and dyes comparable in size and net electric charge with many metabolites and signaling molecules allowing to suggest that the data apply to intercellular electrical signaling and metabolic cell–cell communication *in vivo*. Relatively small ΔV_Rs of ~10 mV can modulate electrical signal transfer and metabolic communication to a large extent through GJs exhibiting V_j-gating asymmetry. Similarly, pulses resembling bursts of APs can block or increase metabolic communication depending on which cell the burst of APs starts.

Transfer of charged molecules is affected by ionophoresis and V_j-gating. Ionophoresis affects cell–cell transfer of charged metabolites independent of Cx type and whether GJ channels are homotypic,

heterotypic or heteromeric. Ionophoresis and V_j-gating can act synergistically or antagonistically on cell-to-cell transfer of the metabolite depending on the sign of its charge and the net J_j direction relative to the orientation of the heterotypic channel. V_j-gating asymmetry of heterotypic GJs in combination with small ΔV_Rs of communicating cells can lead to noticeable J_j–V_j asymmetries. This may explains disputable data on reported earlier directional permselectivity of charged fluorophores [74–76] in heterocellular cell pairs, presumably forming heterotypic GJs. Fig. 7 shows that V_js of ~10 mV or even smaller might render a significant asymmetry of metabolic communication without assuming a presence of directional permselectivity. Our data show that the modified GHK equation used predicts P_γ relatively well for examined dyes. This may not necessarily be true for larger molecules or higher V_js due to: 1) breakdown of ionic independence, 2) electrostatic interaction with the channel's wall, etc.

Since the discovery of V_j-dependent gating of GJ channels it remains unclear a necessity of voltage-gating of GJs expressed in non-excitable cells, such as hepatocytes, astrocytes, keratinocytes, epithelial cells, etc., which do not generate APs that can lead to large V_js. However, as we demonstrate, even relatively small ΔV_Rs of communicating cells can substantially modulate transfer of charged dyes via V_j-gating and ionophoresis, and this effect is augmented in heterotypic GJs. Can such ΔV_Rs be physiologically relevant? V_Rs varies among different cell types in broad ranges exceeding tens of mV under normal conditions, and even more under pathological conditions when cells lose their electrochemical gradients. It has been shown that astrocytes, which are well coupled through GJs, exhibit a wide range of V_Rs from −22 to −82 mV, and exhibit spontaneous changes of their V_Rs under different physiological conditions [73]. Therefore, modulation of metabolic communication by ionophoresis in the absence of V_j-gating can occur in well coupled cell networks, such as the astrocytic network, where small differences in the average membrane potential can modulate the transfer of charged metabolites between different regions of the cell network. A model for ionophoresis of charged molecules through GJ channels showed that a 20 mV difference between the first and last cells, of a linear array of 8 coupled cells, is sufficient to generate a significant gradient of charged molecules [77]. This suggests that ΔV_Rs of ~3 mV, which certainly do not produce V_j-gating, might be enough to generate J_j asymmetries of charged molecules by ionophoresis alone. Numerous studies have shown that pathological conditions such as ischemia, can result in alteration of V_Rs. Depending upon the severity of ischemic conditions, changes in V_R can be far greater than 10 mV [78]. Thus, even in cells that have the same V_R under normal conditions, changes in their network profile or local ischemia can induce ΔV_Rs and consequently modulate metabolic communication by ionophoresis in all types of GJs and, in addition, by V_j-gating if cells are coupled through heterotypic GJs. It is important to note that actual ΔV_R depend on the intrinsic V_Rs of communicating cells, coupling strength and their input resistance.

V_j-gating under physiological conditions can also take place in electrically excitable tissues. It was shown that V_j arising on the front of excitation spread in the heart can dynamically reduce g_j and may play a role in the development of cardiac arrhythmias [79]. Electrical activity during cardiac arrhythmias resembles bursts of APs similar to those in Figs. 1C, 5 and 6 may cause profound changes of g_j and J_j. Similar instances can occur between neurons that express or co-express Cx30.2, Cx36 and Cx45 [16]. Dynamic changes in g_j can also occur when only one of the coupled cells is excitable, as at GJs between neurons and astrocytes, between endothelium and smooth muscle cells in blood vessels, etc. All these systems co-express Cx45 in parallel with Cx31, Cx36, Cx40, Cx43 and/or Cx47 that can form heterotypic GJs exhibiting V_j-gating asymmetry. In the mouse retina, the major rod/cone pathway for visual transmission is mediated by Cx36/Cx45 heterotypic GJ channels formed between ON cone bipolar and AII amacrine cells [80]. In major white matter tracts, where astrocytic Cx30 is absent, astrocytes and oligodendrocytes expressing Cx43 and Cx45, respectively, form Cx43/Cx45 heterotypic channels [31]. In the heart, fibroblasts that are non-excitable express Cx45 [81] among other Cxs and are coupled with cardiomyocytes preferentially expressing Cx43. Fibroblasts, exhibiting relatively small V_Rs, will be more depolarized than cardiomyocytes during the repolarization phase. Thus, most of Cx43/Cx45 GJs should open and cells should be able to exchange metabolites. During APs when the V_m of cardiomyocytes becomes positive, Cx43/Cx45 channels should close resulting in the reduction of g_j, P_j and consequently a 'sink' effect of the fibroblast's network on the excitation of cardiomyocytes, thereby enhancing the safety factor for the spread of excitation in the syncytial network of cardiomyocytes. During the rest of the cardiac cycle, g_j should increase to a degree that fibroblasts might help cardiomyocytes to restore their energetic and ionic balance.

In summary, long-lasting V_js of small amplitude or series of V_j pulses resembling bursts of APs modulate dye transfer with high efficacy suggesting that heterotypic GJs may act as voltage-sensitive regulatory valves for intercellular electrical signaling and metabolic communication. This V_j-dependent modulation of GJC may be important in many aspects of normal physiology during different stages of development and in adults. GJC can be substantially altered under pathological conditions when survival of energetically deficient cells critically depends on metabolic communication with surrounding normal cells.

Acknowledgments

Dr. Michael V.L. Bennett for helpful comments and remarks, and Angele Bukauskiene for excellent technical assistance. This work was supported by NIH Grants, R01NS072238 and RO1HL084464 to F.F.B.

References

[1] V. Verselis, R.L. White, D.C. Spray, M.V. Bennett, Gap junctional conductance and permeability are linearly related, Science 234 (1986) 461–464.
[2] L.R. Wolszon, W.Q. Gao, M.B. Passani, E.R. Macagno, Growth cone "collapse" *in vivo*: are inhibitory interactions mediated by gap junctions? J. Neurosci. 14 (1994) 999–1010.
[3] P. Bedner, H. Niessen, B. Odermatt, M. Kretz, K. Willecke, H. Harz, Selective permeability of different connexin channels to the second messenger cyclic AMP, J. Biol. Chem. 28 (2006) 6673–6681.
[4] V. Valiunas, Y.Y. Polosina, H. Miller, I.A. Potapova, L. Valiuniene, S. Doronin, R.T. Mathias, R.B. Robinson, M.R. Rosen, I.S. Cohen, P.R. Brink, Connexin-specific cell-to-cell transfer of short interfering RNA by gap junctions, J. Physiol. 568 (2005) 459–468.
[5] J. Neijssen, C. Herberts, J.W. Drijfhout, E. Reits, L. Janssen, J. Neefjes, Cross-presentation by intercellular peptide transfer through gap junctions, Nature 434 (2005) 83–88.
[6] A.L. Harris, Emerging issues of connexin channels: biophysics fills the gap, Q. Rev. Biophys. 34 (2001) 325–427.
[7] G. Sohl, K. Willecke, Gap junctions and the connexin protein family, Cardiovasc. Res. 62 (2004) 228–232.
[8] X. Li, N. Kamasawa, C. Ciolofan, C.O. Olson, S. Lu, K.G. Davidson, T. Yasumura, R. Shigemoto, J.E. Rash, J.I. Nagy, Connexin45-containing neuronal gap junctions in rodent retina also contain connexin36 in both apposing hemiplaques, forming bihomotypic gap junctions, with scaffolding contributed by zonula occludens-1, J. Neurosci. 28 (2008) 9769–9789.
[9] F.F. Bukauskas, A. Bukauskiene, V.K. Verselis, M.V.L. Bennett, Coupling asymmetry of heterotypic connexin 45/connexin 43-EGFP gap junctions: properties of fast and slow gating mechanisms, Proc. Natl. Acad. Sci. U.S.A. 99 (2002) 7113–7118.
[10] M. Rackauskas, M.M. Kreuzberg, M. Pranevicius, K. Willecke, V.K. Verselis, F.F. Bukauskas, Gating properties of heterotypic gap junction channels formed of connexins 40, 43 and 45, Biophys. J. 92 (2007) 1952–1965.
[11] G. Sohl, S. Maxeiner, K. Willecke, Expression and functions of neuronal gap junctions, Nat. Rev. Neurosci. 6 (2005) 191–200.
[12] M.M. Kreuzberg, K. Willecke, F. Bukauskas, Connexin-mediated cardiac impulse propagation: connexin 30.2 slows atrioventricular conduction in mouse heart, Trends Cardiovasc. Med. 16 (2006) 266–272.
[13] R. Bruzzone, J.A. Haefliger, R.L. Gimlich, D.L. Paul, Connexin40, a component of gap junctions in vascular endothelium, is restricted in its ability to interact with other connexins, Mol. Biol. Cell 4 (1993) 7–20.
[14] X. Li, J.M. Simard, Connexin45 gap junction channels in rat cerebral vascular smooth muscle cells, Am. J. Physiol. - Heart C. 281 (2001) H1890–H1898.
[15] M.M. Kreuzberg, G. Sohl, J. Kim, V.K. Verselis, K. Willecke, F.F. Bukauskas, Functional properties of mouse connexin30.2 expressed in the conduction system of the heart, Circ. Res. 96 (2005) 1169–1177.
[16] M.M. Kreuzberg, J. Deuchars, E. Weiss, A. Schober, S. Sonntag, K. Wellershaus, A. Draguhn, K. Willecke, Expression of connexin30.2 in interneurons of the central nervous system in the mouse, Mol. Cell. Neurosci. 37 (2008) 119–134.

[17] R. Rozental, A.F. Andrade-Rozental, X. Zheng, M. Urban, D.C. Spray, F.C. Chiu, Gap junction-mediated bidirectional signaling between human fetal hippocampal neurons and astrocytes, Dev. Neurosci.-Basel 23 (2001) 420–431.
[18] R. Bruzzone, S.G. Hormuzdi, M.T. Barbe, A. Herb, H. Monyer, Pannexins, a family of gap junction proteins expressed in brain, Proc. Natl. Acad. Sci. U.S.A. 11 (2003) 13644–13649.
[19] G. Dahl, S. Locovei, Pannexin: to gap or not to gap, is that a question? IUBMB Life 58 (2006) 409–419.
[20] E.J. Furshpan, D.D. Potter, Transmission at the giant motor synapses of the crayfish, J. Physiol. (Lond.) 145 (1959) 289–325.
[21] R. Werner, E. Levine, C. Rabadan Diehl, G. Dahl, Formation of hybrid cell–cell channels, Proc. Natl. Acad. Sci. U.S.A. 86 (1989) 5380–5384.
[22] K.I. Swenson, J.R. Jordan, E.C. Beyer, D.L. Paul, Formation of gap junctions by expression of connexins in *Xenopus* oocyte pairs, Cell 57 (1989) 145–155.
[23] F.F. Bukauskas, R. Vogel, R. Weingart, Biophysical properties of heterotypic gap junctions newly formed between two types of insect cells, J. Physiol. (Lond.) 499 (1997) 701–713.
[24] P. Phelan, L.A. Goulding, J.L. Tam, M.J. Allen, R.J. Dawber, J.A. Davies, J.P. Bacon, Molecular mechanism of rectification at identified electrical synapses in the *Drosophila* giant fiber system, Curr. Biol. 18 (2008) 1955–1960.
[25] L.C. Barrio, T. Suchyna, T. Bargiello, L.X. Xu, R.S. Roginski, M.V. Bennett, B.J. Nicholson, Gap junctions formed by connexins 26 and 32 alone and in combination are differently affected by applied voltage, Proc. Natl. Acad. Sci. U.S.A. 88 (1991) 8410–8414.
[26] G.H. Kalimi, C.W. Lo, Communication compartments in the gastrulating mouse embryo, J. Cell Biol. 107 (1988) 241–255.
[27] G.H. Kalimi, C.W. Lo, Gap junctional communication in the extraembryonic tissues of the gastrulating mouse embryo, J. Cell Biol. 109 (1989) 3015–3026.
[28] D.I. Vaney, R. Weiler, Gap junctions in the eye: evidence for heteromeric, heterotypic and mixed-homotypic interactions, Brain Res. Brain Res. Rev. 32 (2000) 115–120.
[29] G. Sohl, M. Guldenagel, O. Traub, K. Willecke, Connexin expression in the retina, Brain Res. Brain Res. Rev. 32 (2000) 138–145.
[30] J.I. Nagy, R. Dermietzel, Gap Junctions and Connexins in the Mammalian Central Nervous System, in: E.L. Hertzberg (Ed.), Gap junctions, vol. 30, JAI Press, Stamford, 2000, pp. 323–396.
[31] J.I. Nagy, J.E. Rash, Connexins and gap junctions of astrocytes and oligodendrocytes in the CNS, Brain Res. Brain Res. Rev. 32 (2000) 29–44.
[32] E.C. Beyer, L.M. Davis, J.E. Saffitz, R.D. Veenstra, Cardiac intercellular communication: consequences of connexin distribution and diversity, Braz. J. Med. Biol. Res. 28 (1995) 415–425.
[33] P.R. Brink, Gap junctions in vascular smooth muscle, Acta Physiol. Scand. 164 (1998) 349–356.
[34] P.R. Brink, J. Ricotta, G.J. Christ, Biophysical characteristics of gap junctions in vascular wall cells: implications for vascular biology and disease, Braz. J. Med. Biol. Res. 33 (2000) 415–422.
[35] T.W. White, R. Bruzzone, S. Wolfram, D.L. Paul, D.A. Goodenough, Selective interactions among the multiple connexin proteins expressed in the vertebrate lens: the second extracellular domain is a determinant of compatibility between connexins, J. Cell Biol. 125 (1994) 879–892.
[36] C. Elfgang, R. Eckert, H. Lichtenberg-Frate, A. Butterweck, O. Traub, R.A. Klein, D.F. Hulser, K. Willecke, Specific permeability and selective formation of gap junction channels in connexin-transfected HeLa cells, J. Cell Biol. 129 (1995) 805–817.
[37] M.G. Hopperstad, M. Srinivas, D.C. Spray, Properties of gap junction channels formed by Cx46 alone and in combination with Cx50, Biophys. J. 79 (2000) 1954–1966.
[38] I. Bondarev, A. Vine, J.S. Bertram, Cloning and functional expression of a novel human connexin-25 gene, Cell Commun. Adhes. 8 (2001) 167–171.
[39] J. von Maltzahn, C. Euwens, K. Willecke, G. Sohl, The novel mouse connexin39 gene is expressed in developing striated muscle fibers, J. Cell Sci. 117 (2004) 5381–5392.
[40] D. González, J.M. Gómez-Hernández, L.C. Barrio, Molecular basis of voltage dependence of connexin channels: an integrative appraisal, Prog. Biophys. Mol. Biol. 94 (2007) 66–106.
[41] C.I. Foote, L. Zhou, X. Zhu, B.J. Nicholson, The pattern of disulfide linkages in the extracellular loop regions of connexin 32 suggests a model for the docking interface of gap junctions, J. Cell Biol. 140 (1998) 1187–1197.
[42] G. Dahl, R. Werner, E. Levine, C. Rabadan Diehl, Mutational analysis of gap junction formation, Biophys. J. 62 (1992) 172–180.
[43] S. Nakagawa, X.Q. Gong, S. Maeda, Y. Dong, Y. Misumi, T. Tsukihara, D. Bai, Asparagine175 of connexin32 is a critical residue for docking and forming functional heterotypic gap junction channels with connexin26, J. Biol. Chem. 286 (2011) 19672–19681.
[44] S. Haubrich, H.J. Schwarz, F. Bukauskas, H. Lichtenberg-Frate, O. Traub, R. Weingart, K. Willecke, Incompatibility of connexin 40 and 43 Hemichannels in gap junctions between mammalian cells is determined by intracellular domains, Mol. Biol. Cell 7 (1996) 1995–2006.
[45] E.C. Beyer, V.M. Berthoud, The Family of Connexin Genes, in: A.L. Harris, D. Locke (Eds.), Connexins a Guide, Humana Press, New York, 2009, pp. 3–26.
[46] W.G. Liang, C.C. Su, J.H. Nian, A.S. Chiang, S.Y. Li, J.J. Yang, Human connexin30.2/31.3 (GJC3) does not form functional gap junction channels but causes enhanced ATP release in HeLa cells, Cell Biochem. Biophys. (2011).
[47] V.K. Verselis, M.V. Bennett, T.A. Bargiello, A voltage-dependent gap junction in *Drosophila melanogaster*, Biophys. J. 59 (1991) 114–126.
[48] A.L. Harris, D.C. Spray, M.V.L. Bennett, Kinetic properties of a voltage-dependent junctional conductance, J. Gen. Physiol. 77 (1981) 95–117.
[49] F.F. Bukauskas, V.K. Verselis, Gap junction channel gating, Biochim. Biophys. Acta 1662 (2004) 42–60.
[50] F.F. Bukauskas, R. Weingart, Voltage-dependent gating of single gap junction channels in an insect cell line, Biophys. J. 67 (1994) 613–625.
[51] J.A. Madden, P.A. Keller, J.G. Kleinman, Changes in smooth muscle cell pH during hypoxic pulmonary vasoconstriction: a possible role for ion transporters, Physiol. Res. 49 (2000) 561–566.
[52] A. Diarra, C. Sheldon, C.L. Brett, K.G. Baimbridge, J. Church, Anoxia-evoked intracellular pH and Ca2+ concentration changes in cultured postnatal rat hippocampal neurons, Neuroscience 93 (1999) 1003–1016.
[53] M. Obara, M. Szeliga, J. Albrecht, Regulation of pH in the mammalian central nervous system under normal and pathological conditions: facts and hypotheses, Neurochem. Int. 52 (2008) 905–919.
[54] N. Palacios-Prado, F.F. Bukauskas, Heterotypic gap junction channels as voltage-sensitive valves for intercellular signaling, Proc. Natl. Acad. Sci. U.S.A. 106 (2009) 14855–14860.
[55] F.F. Bukauskas, C. Elfgang, K. Willecke, R. Weingart, Heterotypic gap junction channels (connexin26–connexin32) violate the paradigm of unitary conductance, Pflugers Arch. 429 (1995) 870–872.
[56] N. Paulauskas, M. Pranevicius, H. Pranevicius, F.F. Bukauskas, A stochastic four-state model of contingent gating of gap junction channels containing two "fast" gates sensitive to transjunctional voltage, Biophys. J. 96 (2009) 3936–3948.
[57] N. Palacios-Prado, S.W. Briggs, V.A. Skeberdis, M. Pranevicius, M.V. Bennett, F.F. Bukauskas, pH-dependent modulation of voltage gating in connexin45 homotypic and connexin45/connexin43 heterotypic gap junctions, Proc. Natl. Acad. Sci. U.S.A. 107 (2010) 9897–9902.
[58] S. Oh, J.B. Rubin, M.V. Bennett, V.K. Verselis, T.A. Bargiello, Molecular determinants of electrical rectification of single channel conductance in gap junctions formed by connexins 26 and 32, J. Gen. Physiol. 114 (1999) 339–364.
[59] V.K. Verselis, C.S. Ginter, T.A. Bargiello, Opposite voltage gating polarities of two closely related connexins, Nature 368 (1994) 348–351.
[60] M.V. Bennett, Gap junctions as electrical synapses, J. Neurocytol. 26 (1997) 349–366.
[61] C.K. Abrams, M.M. Freidin, V.K. Verselis, T.A. Bargiello, D.P. Kelsell, G. Richard, M.V.L. Bennett, F.F. Bukauskas, Properties of human connexin 31, which is implicated in hereditary dermatological disease and deafness, Proc. Natl. Acad. Sci. U.S.A. 103 (2006) 5213–5218.
[62] N. Palacios-Prado, S. Sonntag, V.A. Skeberdis, K. Willecke, F.F. Bukauskas, Gating, permselectivity and pH-dependent modulation of channels formed by connexin57, a major connexin of horizontal cells in the mouse retina, J. Physiol. (Lond.) 587 (2009) 3251–3269.
[63] A.L. Harris, D.C. Spray, M.V. Bennett, Control of intercellular communication by voltage dependence of gap junctional conductance, J. Neurosci. 3 (1983) 79–100.
[64] G.S. Goldberg, V. Valiunas, P.R. Brink, Selective permeability of gap junction channels, Biochim. Biophys. Acta 1662 (2004) 96–101.
[65] M. Rackauskas, V.K. Verselis, F.F. Bukauskas, Permeability of homotypic and heterotypic gap junction channels formed of cardiac connexins mCx30.2, Cx40, Cx43, and Cx45, Am. J. Physiol. - Heart C. 293 (2007) H1729–H1736.
[66] G.S. Goldberg, A.P. Moreno, P.D. Lampe, Gap junctions between cells expressing connexin 43 or 32 show inverse permselectivity to adenosine and ATP, J. Biol. Chem. 277 (2002) 36725–36730.
[67] Y. Qu, G. Dahl, Function of the voltage gate of gap junction channels: selective exclusion of molecules, Proc. Natl. Acad. Sci. U.S.A. 99 (2002) 697–702.
[68] F.F. Bukauskas, A. Bukauskiene, V.K. Verselis, Conductance and permeability of the residual state of connexin43 gap junction channels, J. Gen. Physiol. 119 (2002) 171–186.
[69] B. Hille, Ionic Channels of Excitable Membranes, Sinauer Associates, Sunderland, MA, 2001.
[70] V. Valiunas, E.C. Beyer, P.R. Brink, Cardiac gap junction channels show quantitative differences in selectivity, Circ. Res. 91 (2) (2002) 104–111.
[71] J.F. Ek-Vitorin, J.M. Burt, Quantification of gap junction selectivity, Am. J. Physiol. Cell Physiol. 289 (2005) C1535–C1546.
[72] F.F. Bukauskas, A. Bukauskiene, M.V.L. Bennett, V.K. Verselis, Gating properties of gap junction channels assembled from connexin43 and connexin43 fused with green fluorescent protein, Biophys. J. 81 (2001) 137–152.
[73] G.M. McKhann 2nd, R. D'Ambrosio, D. Janigro, Heterogeneity of astrocyte resting membrane potentials and intercellular coupling revealed by whole-cell and gramicidin-perforated patch recordings from cultured neocortical and hippocampal slice astrocytes, J. Neurosci. 17 (1997) 6850–6863.
[74] J.L. Flagg Newton, W.R. Loewenstein, Asymmetrically permeable membrane channels in cell junction, Science 207 (1980) 771–773.
[75] S.R. Robinson, E.C. Hampson, M.N. Munro, D.I. Vaney, Unidirectional coupling of gap junctions between neuroglia, Science 262 (1993) 1072–1074.
[76] A. Finkelstein, Gap junctions and intercellular communications, Science 265 (1994) 1017–1018 author reply 1019–1020.
[77] A.T. Esser, K.C. Smith, J.C. Weaver, M. Levin, Mathematical model of morphogen electrophoresis through gap junctions, Dev. Dyn. 235 (2006) 2144–2159.
[78] L. Hyllienmark, T. Brismar, Effect of hypoxia on membrane potential and resting conductance in rat hippocampal neurons, Neuroscience 91 (1999) 511–517.
[79] X. Lin, J. Gemel, E.C. Beyer, R.D. Veenstra, Dynamic model for ventricular junctional conductance during the cardiac action potential, Am. J. Physiol. - Heart C. 288 (2005) H1113–H1123.
[80] S. Maxeiner, K. Dedek, U. Janssen-Bienhold, J. Ammermuller, H. Brune, T. Kirsch, M. Pieper, J. Degen, O. Kruger, K. Willecke, R. Weiler, Deletion of connexin45 in mouse retinal neurons disrupts the rod/cone signaling pathway between AII amacrine and ON cone bipolar cells and leads to impaired visual transmission, J. Neurosci. 25 (2005) 566–576.
[81] P. Camelliti, C.R. Green, I. LeGrice, P. Kohl, Fibroblast network in rabbit sinoatrial node: structural and functional identification of homogeneous and heterogeneous cell coupling, Circ. Res. 94 (2004) 828–835.